Wake galloping energy harvesting in heat exchange systems under the influence of ash deposition

Junlei Wang [a], Chengyun Zhang [a], Guobiao Hu [b, c, *], Xiaowei Liu [d, **], Huadong Liu [a], Zhien Zhang [e], Raj Das [f]

[a] School of Mechanical and Power Engineering, Zhengzhou University, Zhengzhou, 450000, China
[b] School of Civil and Environmental Engineering, Nanyang Technological University, 639798, Singapore
[c] State Key Laboratory of Structural Analysis for Industrial Equipment, Dalian University of Technology, Dalian, 116024, China
[d] State Key Laboratory of Coal Combustion, Huazhong University of Science and Technology, Wuhan, 430074, China
[e] Department of Chemical and Biomedical Engineering, West Virginia University, Morgantown, WV, 26506, USA
[f] School of Engineering, RMIT University, GPO Box 2476, Melbourne, VIC, 3001, Australia

ARTICLE INFO

ABSTRACT

Since the fluid flows in heat exchange systems contain hydrokinetic energies, flow-induced vibration (FIV) energy harvesting technology can be potentially applied to collect electrical energy. Different from the applications in traditional scenarios, cylinder bluff bodies implemented in the heat exchange systems will inevitably suffer from ash deposition. This study proposes a wake galloping energy harvester to be used in heat exchange systems and focuses on investigating the effects of different ash deposition types on the energy harvesting performance. According to different ash deposition types, bell-shaped and horn-shaped cylinder bluff bodies are designed to consider the ash deposition effect. Wind tunnel experiments are conducted to investigate the performance of the wake galloping piezoelectric energy harvester (PEH) with different upstream ash deposit cylinders, at various space distances and under different wind speeds. The experimental results reveal that compared to the horn-shaped cylinder, the bell-shaped cylinder is more beneficial for energy harvesting. Among all tested cases, the optimal configuration is determined: the upstream cylinder is attached by bell-shaped ash deposition; and the space ratio between the upstream and the downstream cylinders is 1.5. The threshold wind speed of the optimal configuration is reduced and the maximum voltage output is improved by over 111%. It is learned that the two types of upstream ash deposit cylinders can both cause the quenching phenomenon to deteriorate the performance of the energy harvester. Guidelines based on the experimental results are provided to avoid the occurrence of the quenching phenomenon. Computational fluid dynamics (CFD) studies are conducted to reveal the underlying mechanisms to explain the experimental results. The CFD results corroborate that different ash deposit cylinders produce different wake vortices and the flow pattern changes with the space distance, which determines the dynamic response of the downstream cylinder.

© 2022 Elsevier Ltd. All rights reserved.

1. Introduction

With the fast development of wireless sensor networks (WSNs), wearable and portable microelectronic products, harvesting energy from the ambient environment has been proposed as a potential solution to provide sustainable power supplies for those devices [1,46,63]. As a kind of clean and renewable energy, winds are widely accessible natural sources for energy harvesting [52,54]. Unlike the traditional method of using turbines for large-scale power generation, innovative wind energy harvesting systems with compact dimensions have been developed for low-power consumption devices [3,4,51]. Based on various flow-induced vibration (FIV) phenomena including vortex-induced vibration (VIV) [5,55,60], galloping [48,53], flutter [7], and wake galloping [8],

wind energy harvesters first convert hydrokinetic energy into vibration energy. Subsequently, four commonly used energy conversion mechanisms, namely electrostatic [9], electromagnetic [10,11,49], piezoelectric [12,57,58], and triboelectric [13,61,62] transductions, can be employed to convert the mechanical energy into electrical energy. To date, various energy harvesters have been designed based on different FIV phenomena and transduction mechanisms [47,56,59]. Bernitsas et al. [14] first proposed the concept of VIV-based aquatic clean energy harvesting (VIVACE). They successfully converted the water flow energy into electricity using the VIV mechanism. Akaydin et al. [15] developed an VIV-based energy harvester and evaluated its output performance through wind tunnel experiments. Yang et al. [16] compared the performance of a galloping-based piezoelectric energy harvester (PEH) using bluff bodies with various cross-section profiles. They concluded that a square-sectioned bluff body usually demonstrates the best performance. Bryant and Garcia [17] designed a flutter-based aeroelastic energy harvester and estimated its voltage output. Numerous theoretical analyses and experimental studies have revealed the aerodynamic instability characteristics related to those FIV phenomena [18,19]. It is learned that galloping and flutter are divergent oscillations, and the vibration responses increase sharply with the increase of the wind speed, resulting in high-amplitude oscillations and thereby considerable power outputs. However, the threshold wind speeds of them are relatively high, making them difficult for low wind speed energy harvesting. VIV is a type of self-excited oscillation that often undergoes an intense vibration in the synchronization region (known as the lock-in range) as the Strouhal vortex shedding frequency approaches the natural frequency of the energy harvester [20]. Lv et al. [21] provided a comprehensive review of using nonlinear oscillators in hydrokinetic energy harvesting. Harvesting energy from alternating lift technology (ALT) was introduced and nonlinear flow induced oscillation (FIO) was specially emphasized. As compared to galloping and flutter, VIV often takes place at relatively low wind speed, is more suitable for low wind speed energy harvesting. However, the drawback of a VIV-based energy harvester is that the effective wind speed range for energy harvesting is narrow.

Wake galloping has increasingly attracted more attention in recent years. It is defined as the divergent vibration of the downstream cylinder caused by the wake generated after the upstream cylinder, such as the bridge cables or overhead transmission lines in the wind [22]. Jung et al. [23] used wake galloping to harvest electromagnetic energy for the first time, and validated the proposed system through experiments. Afterwards, Usman et al. [24] proposed a novel piezoelectric energy harvesting system based on the wake galloping phenomenon. The proposed system could operate in a wider range of wind speeds in the wind tunnel tests. The optimal space distance between the two cylinders was determined. However, the authors did not explore the influence of the bluff body shape on the performance of the energy harvesting and lack an explanation of the underlying mechanism of wake galloping. Zhou and Wang [25] developed a modified design by installing two identical VIV-PEHs in series in the wind tunnel. The experimental and numerical results showed that the effective wind speed range and output power amplitude of the system were 2.67 times and 6.79 times that of a single VIVPEH. Abdelkefi et al. [26] proposed to place a circular cylinder upstream of a galloping piezoelectric energy harvester (GPEH) with the square cylinder for wake galloping. The results revealed that the wake galloping could enhance the performance of a GPEH: the effective wind speed range for energy harvesting was significantly broadened. By introducing nonlinearity, Alhadidi and Daqaq [27] exploited a bistable restoring force to enlarge the steady-state bandwidth of a wake galloping energy harvester. Inspired by the galloping of iced

conductors, Yan et al. [28] investigated the energy harvesting from wake galloping of downstream crescent-shaped and D-shaped cylinders. The results showed that the wake effect of the upstream fixed circular cylinder could enhance the performance of the downstream VIVPEH. The power density of the wake galloping energy harvester with the iced-conductor cylinder is about 63 times that of the wake galloping energy harvester with a classic circular cylinder. Tamimi et al. [29] investigated the influence of an upstream cylinder with different cross-section on the performance of wake galloping energy harvesting system. The results show that the diamond oscillator is more beneficial to energy harvesting than the sharp edge square oscillator. Yan et al. [30] developed a wind energy harvester with upstream and downstream interference to collect highway wind resources. They found that the upstream spacing has a greater impact on the harvesting power than the downstream spacing. Liu et al. [31] proposed that by placing a fixed double-plate structure upstream of the bluff body, the output voltage of the energy harvester was increased by 12 times. Most of these studies only analyze the performance of the harvester, but there are few studies on underlying flow physics and vortex interaction dynamics of wake galloping. There is a need to explore what kind of interactions between the flow and the structure trigger the complex wake galloping phenomena. Wake galloping may occur at relatively low wind speeds, with a large but limited amplitude. It exhibits a wider wind speed range than VIV for effective energy harvesting. Wake galloping might be more appropriate for energy harvesting systems than VIV, galloping and flutter [32].

FIV-based small energy harvesters have been widely used in various fields, *e.g.*, civil, marine, and aerospace engineering [33,50]. Abdelkefi [34] reviewed various applications of small-scale energy harvesters in different disciplines. These harvesters can be deployed in many locations, *e.g.*, urban high-rises, ventilation outlets, ducts of buildings, bridges, rivers, rails and aircraft structures [35,36]. In thermal engineering, the heat exchanger in the boiler is a crucial device for energy saving and heat transfer [37]. However, when the fly-ash particles in the flue gas impact the tube, a portion of particles will deposit on the surface of the tube and deteriorate the heat transfer performance. Extensive research has been carried out to reduce fly-ash deposition on the tube for improving the heat transfer efficiency [38]. The ash formation and deposition modelling processes in coal and biomass-fired boilers are reviewed by Cai et al. [39]. It was pointed out that the ash deposition phenomenon is an inevitable problem.

From another point of view, the ash deposition phenomenon may have a positive effect on energy harvesting. This paper proposes to deploy aeroelastic energy harvesters in flue gas heat exchanger devices for the first time. These harvesters are expected to power small electronic devices implemented in the boiler for possibly realizing self-powered health monitoring. Unlike traditional FIV-based energy harvesters implemented in other scenarios, the cross-sectional shape of the heat exchange tube will change due to the influence of ash deposition. According to the literature [40], there are two main types of ash deposition on the tube, namely, bell-shaped and horn-shaped ash deposition. Fig. 1 presents the ash deposits on two parallel circular tubes. The bell-shaped ash deposition is formed on the windward side of the first tube. Due to the influence of the wake of the upstream tube, horn-shaped ash deposition is formed on the windward side of the second tube. Considering that a suitable scenario for wind energy harvesting readily exists in a heat exchanger device, we are inspired to place a conventional VIVPEH with a circular cylinder downstream of the first tube or the second tube to use wake galloping phenomenon for energy harvesting. The upstream cylinder with different cross-sectional shapes has a huge impact on the energy harvesting
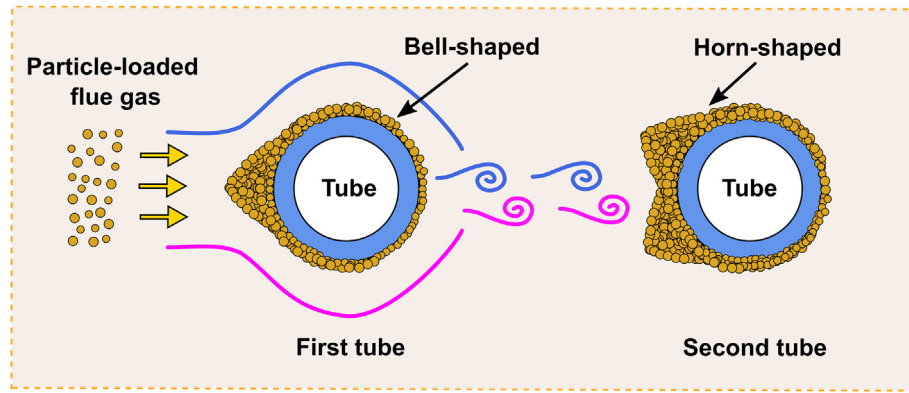
Fig. 1. Schematic of two different types of ash deposition formed on the tube in the heat exchange systems.

efficiency. Most of the existing studies have not attempted to apply harvesters to a heat exchanger device and have not considered the effect of ash deposition. The flow dynamics and vortex interaction dynamics in the wake galloping phenomenon of two series cylinders have not been explored in detail. There is a crucial need for a comprehensive study to determine the impact of bell-shaped and horn-shaped ash deposition on the performance of energy harvesters. The study presented in this work aims to explore the influence of two shapes of upstream ash deposit cylinders on the performance of wake galloping PEHs through wind tunnel experiments. Various space distances between the two cylinders are also investigated. The experimental results are analyzed by fluid force. A comprehensive CFD simulation study is carried out to reveal the underlying mechanism to explain the experimental results, which is an original contribution of this paper. The research in this paper provides some guidelines for the application of FIV-based small-scale energy harvesters in the field of thermal engineering.

2. Design concept and experimental setup

This section introduces the design concept of the proposed energy harvester and the experimental setup for testing its performance. As shown in Fig. 2 (a), an ash deposit cylinder is placed in parallel with and at the upstream of a conventional cylinder. In the proposed system, the upstream ash deposit cylinder is supported by a rigid rod. The downstream circler cylinder is elastically mounted on a cantilever beam. A piezoelectric transducer is bonded on the cantilever beam near its fixed end. When the fluid flows through the upstream cylinder, the wake vortices will be generated to interfere with the downstream cylinder, resulting in a complicated fluid-structure interaction. Obviously, the cross-sectional shape of the upstream cylinder affects the wake vortices formed behind it, thus the dynamics of the downstream cylinder.

As mentioned in the literature [40], the cross-sectional shapes of the common ash deposit tubes in boilers can be classified into bell-shaped and horn-shaped types. As shown at the right-hand side of Fig. 2(a), the bell-shaped and horn-shaped cylinders are designed to simulate the ash deposited tubes. To be more specific, an ornament in the shape of a semi-ellipse is attached to the upstream cylinder to simulate the ash deposition. The bell-shaped cylinder is achieved by adding a semi-ellipse to a conventional cylinder, and the horn-shaped cylinder is obtained by adding two semi-ellipses. The diameter of the cylinder is D. The major and minor axes of the ellipse are D and $D/2$. Note that the major axis of the semi-ellipse attached to the bell-shaped cylinder is parallel to the windward direction. The major axes of the two semi-ellipses attached to the

horn-shaped cylinder are perpendicular to each other and symmetrically distributed on both sides of the cylinder. The effect of the distance between the cylinders on the energy harvesting performance is investigated. L represents the distance between the center axes of the two cylinders. In the experiment, a series of distances ($L/D = 1.5, 2.0, 2.5, 3.0, 3.5, 4.0, 4.5, 5.0$) are tested. The selection of the range of L/D is to comprehensively consider the experimental conditions and workload to ensure effective study of the wake phenomenon.

Fig. 2(b) and (c) present the manufactured prototypes of the bell-shaped cylinder and the horn-shaped cylinder. The upstream and downstream cylinders are of the same dimension, and both are made of foam. The diameter D and height H of the cylinder are 32 mm and 118 mm. The cantilever beam is made of aluminum. The length, width, and thickness of the aluminum beam are 200 mm, 25 mm, and 0.5 mm. The internal capacitance of the piezoelectric transducer (PZT-5) is 24.44 nF. The entire piezoelectric energy harvesting system is fixed on an aluminum frame and placed in an open wind tunnel for testing.

Fig. 3 presents the experimental setup. The wind tunnel is made of plexiglass and has a circular cross-section with a diameter and length of 0.4 m and 5 m. The honeycomb-like structures inside the wind tunnel are used to stabilize the incoming wind. The wind speed is controlled by adjusting the rotational speed of a draught fan. The test wind speed (U) is some discrete value, and range is from 0.87 m/s to 3.19 m/s. The voltage signal generated by the piezoelectric transducer and the displacement of the downstream cylinder are measured, respectively, using a digital oscilloscope (ISDS220B) with a vertical resolution of 8 bit and a laser displacement sensor (Panasonic: HG - C1400) with a resolution of 300 μm. At each wind speed, the dynamic responses of the downstream cylinder are recorded for a sufficiently long duration to ensure that they reach steady states. The RMS value of voltage (V_{rms}) and the maximum value of the displacement (y_{max}) are determined based on the steady-state response.

A free-decay test can identify the physical parameters of the vibratory system. The natural frequency of the system is 8.14 Hz, and the damping ratio is 1.22%. The Scruton number (S_c) of the vibrating model of the energy harvester is 2.42 ($S_c = 2m(2\pi\zeta)/\rho D^2$, m: mass per length, ζ: damping ratio, ρ: fluid density). We repeated the wind tunnel test of the conventional VIVPEH without the upstream cylinder five times prior to the subsequent comparison studies. The maximum relative standard deviation (RSD) of the repeated test voltage results over the lock-in region is less than 2%. Therefore, the reproductivity of the test is verified.
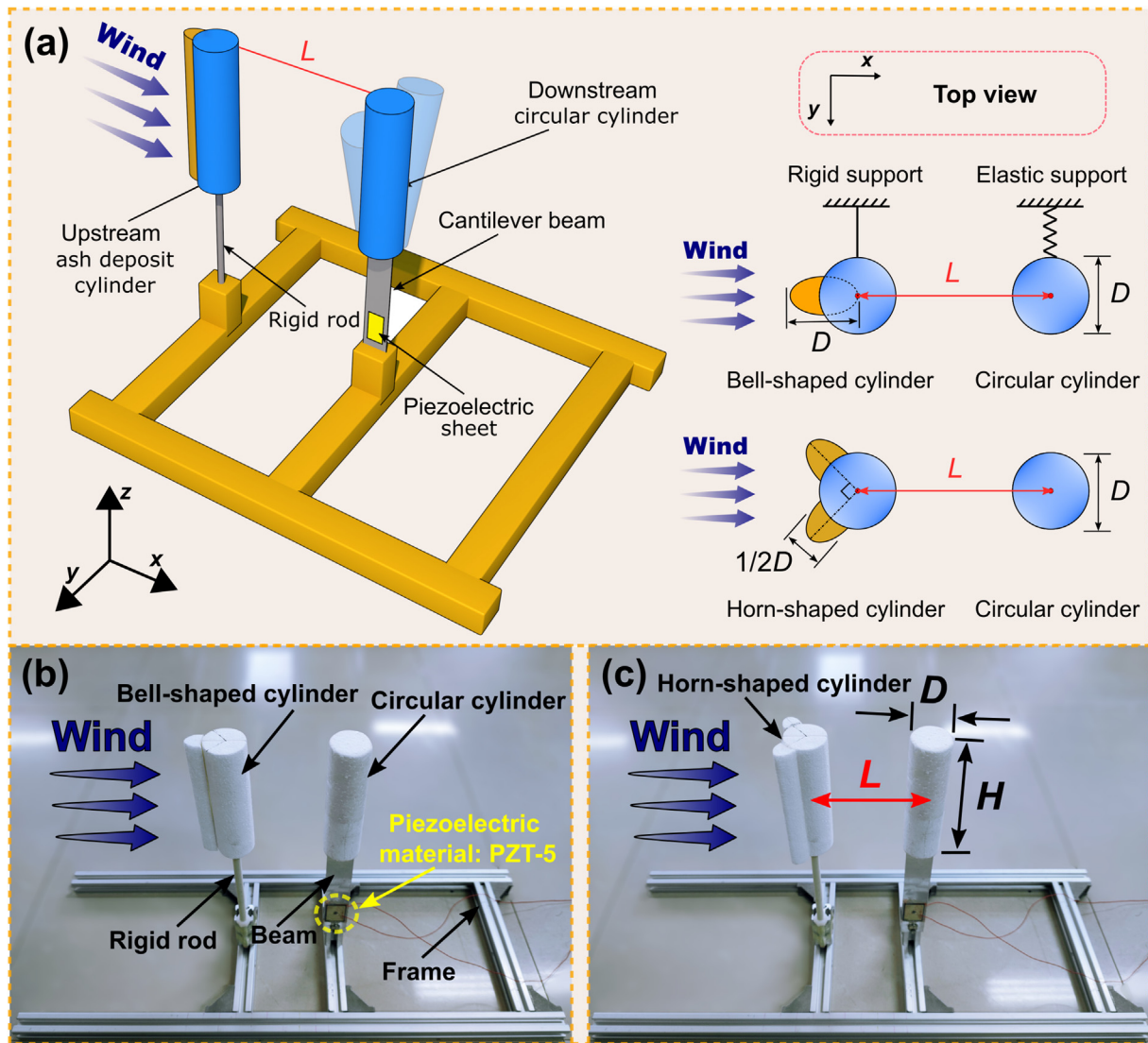
Fig. 2. Schematics of the conceptualized model: (a) 3D schematic and top view; The manufactured prototype with the upstream (b) bell-shaped cylinder and (c) horn-shaped cylinder.

3. Experimental results and discussion

3.1. Energy harvesting performance evaluation

Assuming that a bell-shaped ash deposition is formed on the upstream cylinder, Fig. 4 presents the root-mean-square (RMS) open-circuit voltage V_{rms} and the maximum displacement y_{max} of the energy harvester implemented at the downstream. The space ratio L/D is varied from 1.5 to 5.0 to investigate its influence. The experimental results of a conventional VIVPEH, $i.e.$, the energy harvester without the upstream cylinder, are also presented for comparison. The results clearly show that the performance of the conventional VIVPEH is significantly affected after introducing the upstream bell-shaped cylinder. A typical wake galloping behavior is observed when the bell-shaped cylinder is placed very close to the downstream cylinder ($i.e.$, $L/D = 1.5$). To be more specific, the V_{rms} curve and y_{max} curve increase logarithmically with the increase of wind speed. The voltage amplitude growth is very fast in the early stage, but becomes slower in the later stage. This is similar to the experimental results of wake galloping between two identical circular cylinders reported by Jung et al. [23]. At the highest wind

speed of 3.19 m/s, when $L/D = 1.5$, the maximum voltage output from the piezoelectric transducer reaches 13.43 V, which is 111.83% higher than that of the conventional VIVPEH ($i.e.$, 6.34 V). The upstream bell-shaped cylinder at $L/D = 1.5$ has a threshold wind speed (the lowest wind speed to activate the energy harvester) of 1.14 m/s, which is lower than that of the conventional VIVPEH ($i.e.$, 1.28 m/s). As the space ratio is a little larger, $e.g.$, $L/D = 2.0–3.0$, the generated voltage and the vibration displacement are also remarkably increased compared to the conventional VIVPEH. Different from $L/D = 1.5$, the V_{rms} curve and y_{max} curve exhibit the VIV phenomenon. With the increase of the wind speed, the voltage/displacement amplitude first increases then decreases. The voltage and displacement at high wind speeds show a downward trend: the larger the space ratio, the faster the decline. After this drop, as the wind speed increases further, the voltage and displacement remain almost unchanged.

Interestingly, the voltage and displacement of $L/D = 3.0–4.0$ gradually increase, but the threshold wind speed gradually increases. At larger space ratios ($i.e.$, $L/D = 3.5$ and 4.0), the voltage and displacement suddenly decrease again. This can be expected that the effect of the upstream bell-shaped cylinder is weakened
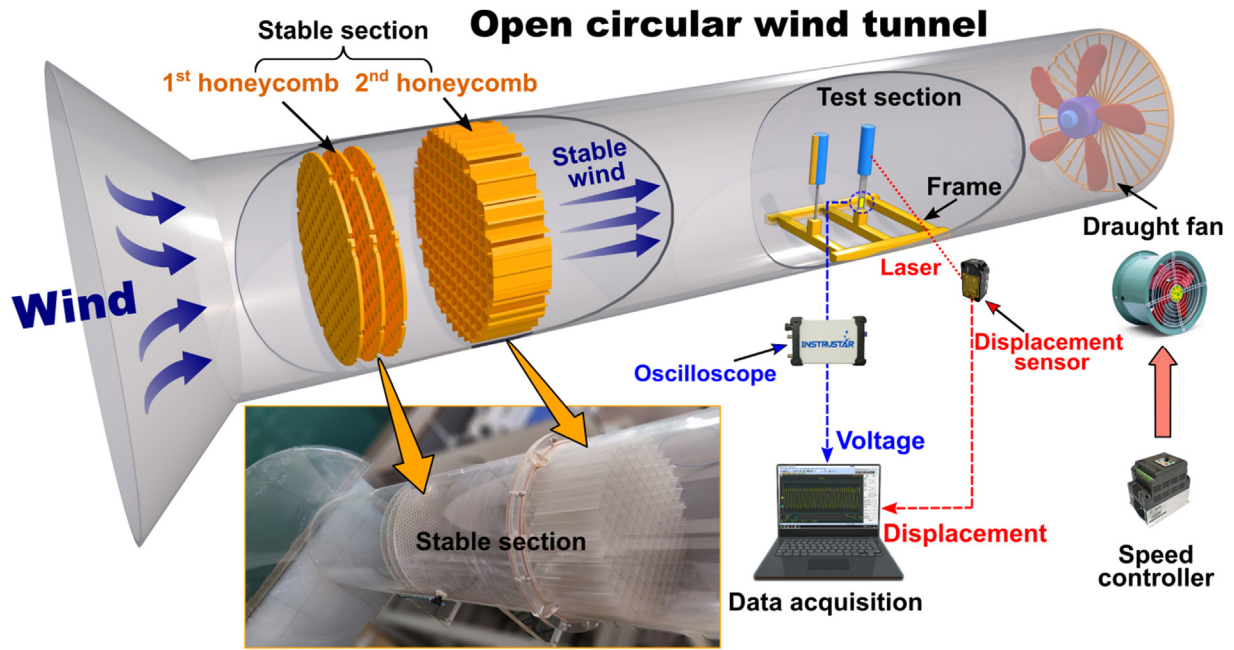
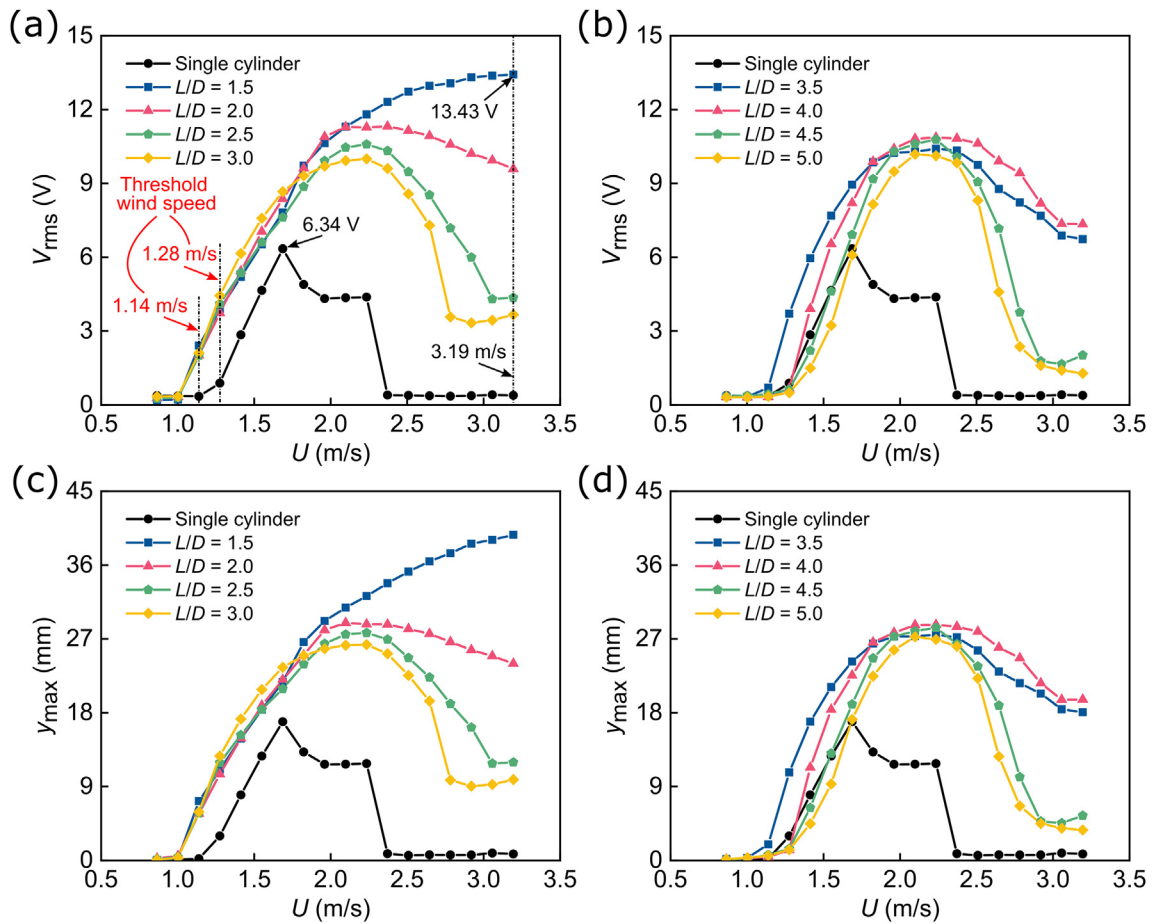**Fig. 3.** The experimental set up.

Fig. 4. Voltage and displacement responses of the downstream energy harvester under the influence of the upstream bell-shaped cylinder.

with an increasing space ratio. In conclusion, since the voltage at this space ratio is significantly larger than those in other cases, the optimal space ratio L/D seems to be around 1.5. Though in the left part of the lock-in range, the voltage/displacement response at some space ratios (*i.e.*, $L/D = 4.0-5.0$) is smaller than that of the conventional VIVPEH. Overall speaking, the larger maximum voltage output and the wider effective wind speed range indicate that all the configurations with the existence of the upstream bell-shaped cylinder outperform the conventional VIVPEH.

In the second case, we place the conventional VIVPEH at the downstream position of a horn-shaped cylinder. Fig. 5 presents the RMS open-circuit voltage V_{rms} and the maximum displacement y_{max} of the energy harvester. In general, all configurations still exhibit VIV characteristics: the voltage amplitude first increases then decreases. When $L/D = 1.5$, the dynamic responses of the energy harvesters with and without the upstream horn-shaped cylinder are almost the same. When L/D increases from 1.5 to 2.5, the maximum V_{rms} and y_{max} gradually decrease. However, when L/D increases from 2.5 to 5.0, the maximum V_{rms} and y_{max} increase. Different from the previous case when the upstream cylinder has a bell-shaped ash deposition, the optimal space ratio (L/D) to achieve the maximum V_{rms} is around 4.5. The maximum voltage output of $L/D = 4.5$ is about 9.90 V, which indicates a 56.15% improvement as compared to the conventional VIVPEH without the upstream horn-shaped cylinder. It is worth noting that the range of $L/D = 2.5-3.0$ is the quenching region that will be discussed in the next section, the performance of the energy harvester is significantly inferior to that of a single cylinder. In the left part of the VIV lock-in range, when

there exists the upstream horn-shaped cylinder, regardless of the space ratio, the V_{rms} and y_{max} are always smaller than those of the conventional VIVPEH. On the whole, the lock-in region gradually moves toward higher wind speeds as the space ratio L/D increases. We can conclude that the existence of the upstream horn-shaped cylinder limits the performance of the VIVPEH. The energy harvesting performance at lower wind speeds always deteriorates. The voltage output amplitude can be significantly improved only at the specific higher wind speeds and certain space ratios.

When bell-shaped and horn-shaped ash depositions are formed on the upstream cylinders, Fig. 6 presents the voltage output of the energy harvester versus the wind speed and the distance ratio L/D. When the ash deposition is in different shapes, the voltage evolution under the influences of the wind speed and the distance ratio L/D is different. From Fig. 6(a) and (b), it can be seen that when the upstream cylinder is attached by the bell-shaped ash deposition and the space distance to the downstream cylinder is small (*i.e.*, L/D is around 1.5), the energy harvester exhibits wake galloping behavior. As the upstream cylinder is deployed farther away, *i.e.*, L/D increases, the dynamic behavior of the downstream energy harvester gradually transforms to VIV. According to the results revealed in Fig. 6(c) and (d), when the upstream cylinder is attached by the horn-shaped ash deposition, the VIV phenomenon always exhibits regardless of the tuning of the space ratio within the investigated range. Compared to the case of horn-shaped ash deposition, the bell-shaped ash deposition formed on the upstream cylinder can lead to a wider effective wind speed range for energy harvesting. Interestingly, when the space ratio L/D is between
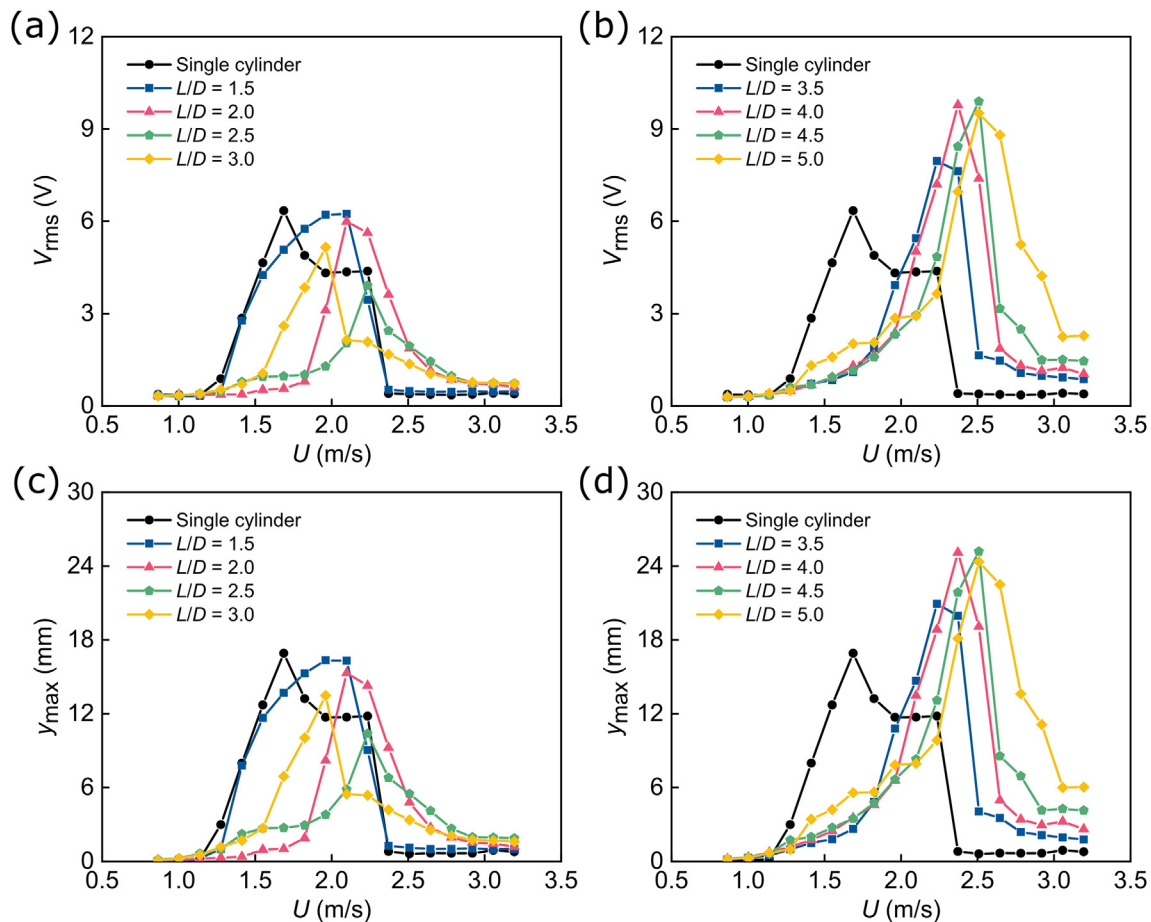

Fig. 5. Voltage and displacement responses of the downstream energy harvester under the influence of the upstream horn-shaped cylinder.
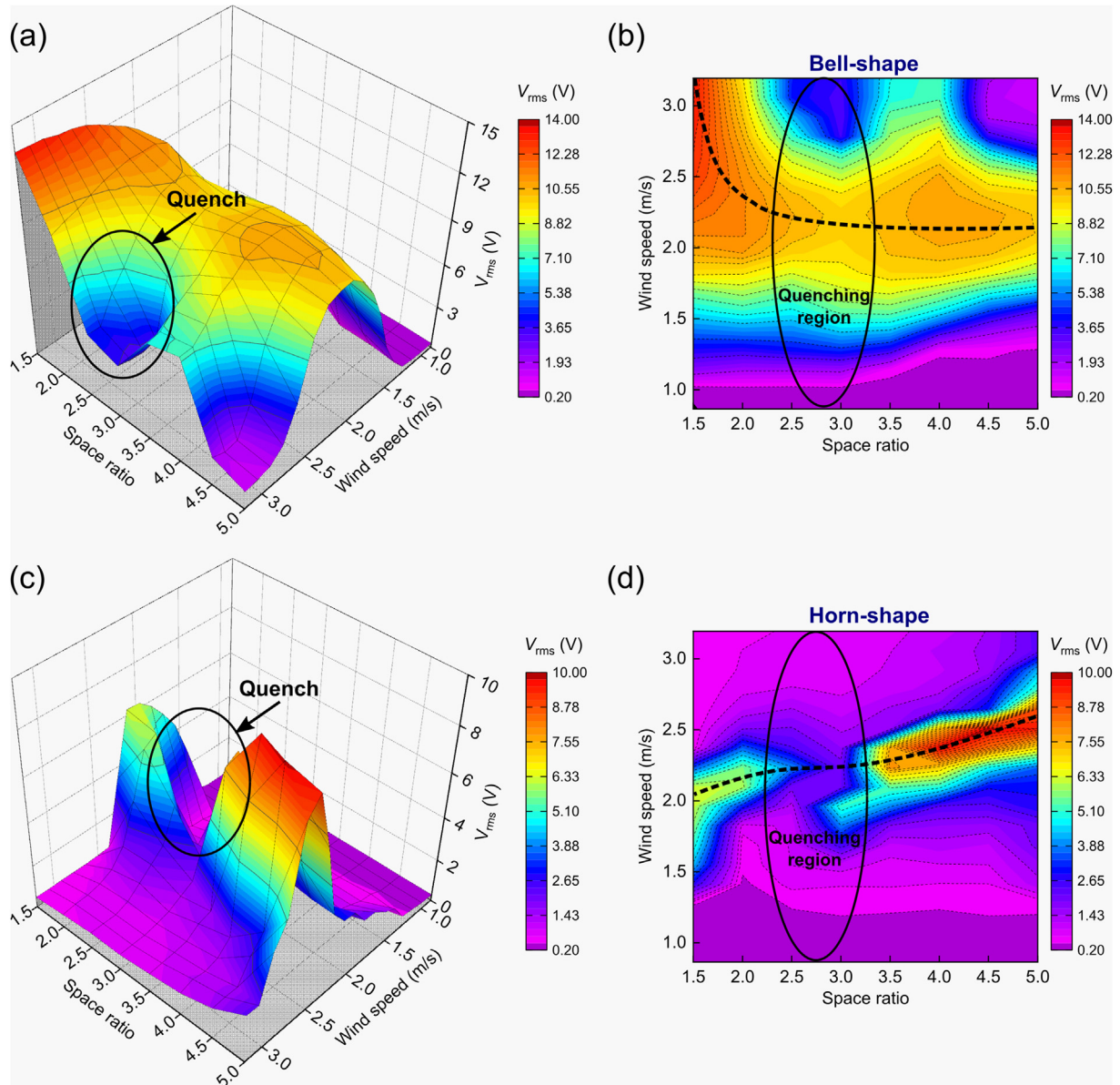
Fig. 6. Surface plot and contour plot of voltage for energy harvester with different upstream ash deposit cylinders: (a) and (b) the bell-shaped cylinder; (c) and (d) the horn-shaped cylinder.

2.5−3.0, regardless of the wind speed, the voltage generated by the energy harvester in the two cases reaches the minimum. The response valleys formed in Fig. 6 can be explained by the quenching behavior [41]. The quenching phenomenon takes place due to the cancellation of multiple excitations [42]. In the cases presented in this study, the multiple excitations refer to wake galloping and VIV. When the space ratio exceeds the quenching region, the response decay effect disappears, and the voltage output of the energy harvester becomes considerably large. The dashed backbone line depicted in Fig. 6 represents the wind speed when the local maximum voltage is attained, indicating the most suitable condition for benefiting energy harvesting. For the case with bell-shaped ash deposition, the optimal wind speed decreases as the space ratio increases. While, for the case with horn-shaped ash deposition, the optimal wind speed increases as the space ratio increases. By following the guideline (*i.e.*, dashed backbone line) to tune the system parameters, a considerable voltage output can be expected,

except for the quenching region in the case of the horn-shaped ash deposition.

3.2. Quenching phenomenon analysis

The presence of the upstream cylinder affects the flow field around the downstream cylinder, thereby alters the aerodynamic force applied on it. As known that the vortex-induced force acting on the downstream cylinder can be described by the lift (C_L) and drag (C_D) coefficients. According to the conclusion in Ref. [43], when two cylinders are tandem in cross-flow, the lift and drag coefficients change with the space ratio, as shown in Fig. 7. It is worth mentioning that the lift and the drag forces acting on the single cylinder strongly depend on the Reynolds number. The Reynolds number of the flow investigated in the experiments approximately ranges from 1.8e3 to 6.9e3. The data presented in Fig. 7 are obtained under the flow condition $Re \approx$ 5e4. The results in
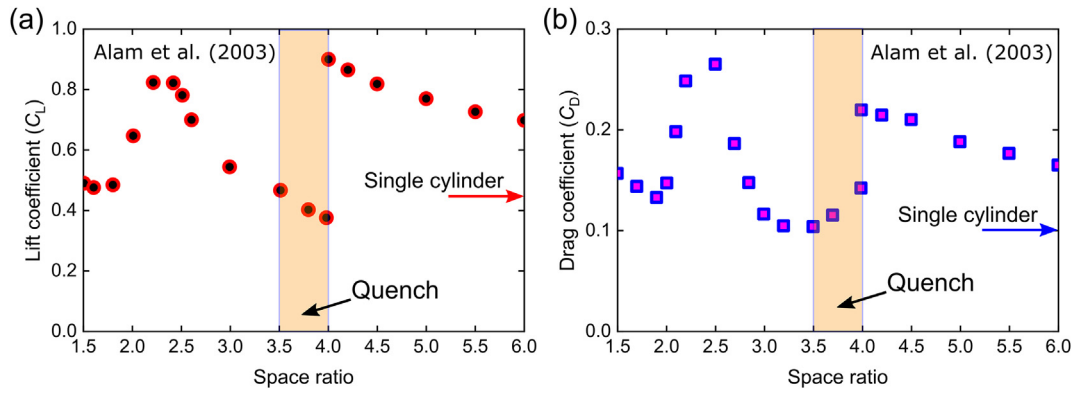
Fig. 7. Variation in fluid forces with an increase in space ratio L/D: (a) lift coefficient, C_L; (b) drag coefficient, C_D. Data from Ref. [43].

Fig. 7 can be used to qualitatively explain the cases presented in this study. As revealed in Fig. 7, when the space ratio is small (*i.e.*, $L/D = 1.5-2.0$), the lift coefficient increases, and the drag coefficient decreases, which results in a higher oscillation amplitude of the energy harvester. This can explain the higher voltage output from the energy harvester when the distance between the upstream and the downstream cylinders is small. Subsequently, over the range of $L/D = 2.5-3.5$, the lift and drag coefficients have almost the same varying trend. Note that when the space ratio is $L/D = 3.5-4.0$, the lift coefficient gradually decreases and becomes smaller than those of a single cylinder. While the drag coefficient gradually increases and becomes larger than those of a single cylinder. The bistable flow reported by Alam and Meyer [44] occurs at the critical space ratio $L/D = 4.0$. The lift and drag coefficients at the critical spacing drastically increase. This can be used to explain the occurrence of the quenching phenomenon.

3.3. Mechanism analysis based on CFD simulation

Computational fluid dynamic (CFD) simulations based on the XFlow platform (Dassault, co.,) are performed to further reveal the underlying mechanisms behind the phenomena mentioned above. To ensure the convergence of the numerical calculation and the accuracy of subsequent simulation results, a fixed two-dimensional single circular cylinder placed in an incoming flow is first simulated. In the convergence study, three different lattice resolutions ($D/8$, $D/16$, $D/32$) are set, which are referred to as coarse, medium, and refined sizes, respectively. The element numbers of the three lattice models are 51,700, 205,512, and 818,388, respectively. Fig. 8 presents time-history curves of the drag coefficient using three different lattice sizes. Table 1 lists the mean values of the drag coefficient C_D and the RMS values of the lift coefficient C_{Lrms}. It can be found that the computational results of C_D and C_{Lrms} gradually converge, and the divergences decrease progressively. The convergence study indicates that using the medium lattice size is sufficient to achieve satisfactory accuracy. Therefore, the subsequent CFD simulations use the medium lattice size to balance computational cost and accuracy.

Fig. 9(a)-(e) demonstrate the vorticity contours to illustrate vortex shedding processes. In the figure, T represents the Strouhal vortex shedding period corresponding to each case. By comparing Fig. 9(a)−(c), it is found that when the upstream cylinder is attached by a bell-shaped ash deposition, for $L/D = 1.5$ and 5.0, the near wake of the downstream cylinder is more violent than that of a single cylinder. The vortex shedding process after the single cylinder exhibits in a stable "2S" mode [45]. When $L/D = 1.5$, the two cylinders are close to each other. The downstream cylinder is like
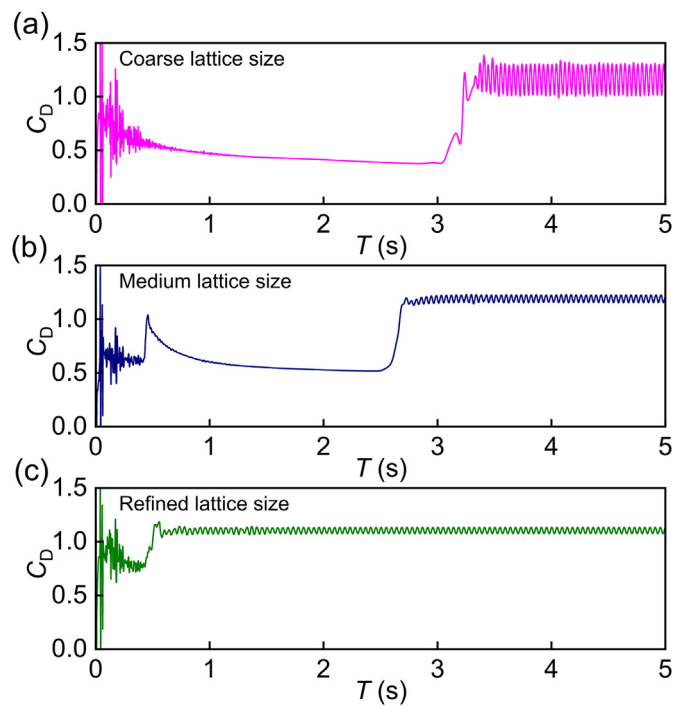

Fig. 8. The time history curves of the drag coefficient simulated by CFD: (a) coarse size; (b) medium size; (c) refined size.

Table 1
The drag coefficient C_D and the root mean square (RMS) values of the lift coefficient C_{Lrms} obtained by different sized lattice models.

Size	C_D	C_{Lrms}
Coarse	0.739	0.471
Medium	1.035	0.339
Refined	1.104	0.334

an extension of the upstream cylinder, causing the downstream cylinder to be wrapped inside the vortex formation regime of the upstream cylinder. In fact, the two cylinders are transformed into a single slender bluff body resembling an elliptical cross-section. The vortex shedding pattern behind it exhibits the "P + S" mode, resulting in the wake galloping phenomenon with a large oscillation amplitude.

Given $L/D = 5.0$ in Fig. 9(c), the vortices generated behind the upstream cylinder alternately adhere to the upper and lower
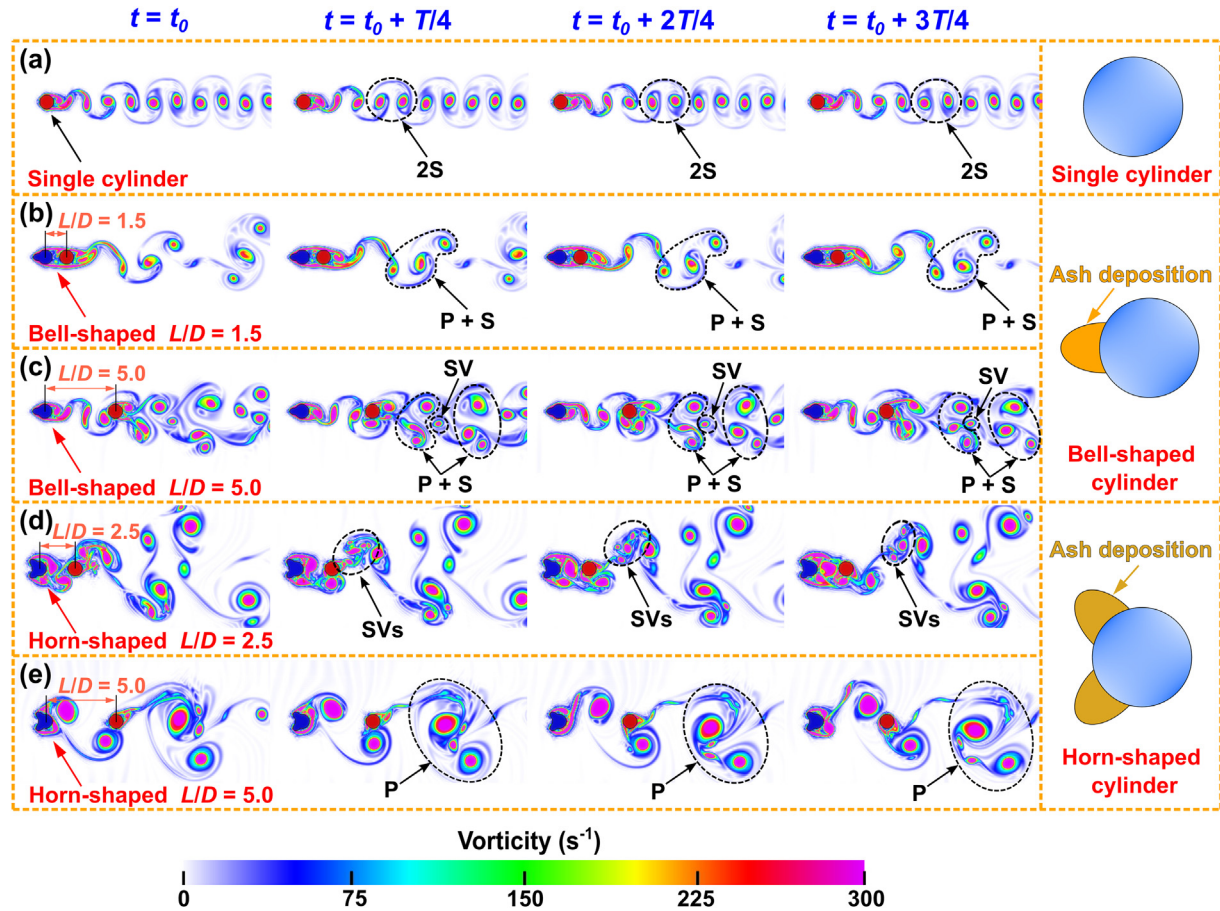
Fig. 9. Vorticity contours obtained from CFD simulation to illustrate the vortex shedding processes: (a) the single cylinder; (b) the bell-shape cylinder for $L/D = 1.5$; (c) the bell-shape for $L/D = 5.0$; (b) the horn-shape cylinder for $L/D = 2.5$; (b) the horn-shape cylinder for $L/D = 5.0$.

surfaces of the downstream cylinder. The vortex shedding process in the case when $L/D = 5.0$ still displays the "P + S" mode and becomes more unstable as compared to the case when $L/D = 1.5$. A small vortex (SV) appears between every two adjacent "P + S" modes and weakens the overall excitation of the downstream cylinder. This provides the potential explanation for why the performance of the case when $L/D = 5.0$ to be inferior to that of the case when $L/D = 1.5$, as indicated in Fig. 4. As observed in Fig. 9(d) and (e), the size of the vortex generated behind the horn-shaped cylinder is significantly larger than that behind the bell-shaped cylinder. For the horn-shaped cylinder at $L/D = 2.5$, the distance between the upstream and downstream is relatively close, which causes the vortex generated behind the upstream cylinder not to form a complete body, that is, the aborted (incomplete) vortex. These aborted vortices interact with the shear layer and reattach to the surface of the downstream cylinder, which greatly affects the shedding of the vortex behind the downstream cylinder, causing the vortex near the back surface of the cylinder to become several fragmented and unreliable SVs. This greatly limits the vibration of the downstream cylinder, resulting in a smaller voltage output into the quenching region displayed in Fig. 6. Note that for $L/D = 2.5$, the downstream cylinder is located outside the upstream vortex formation region, and the shedding vortex behind the horn-shaped cylinder is a stable and complete body. The alternating full vortices from the upstream cylinder strike on the downstream cylinder and embrace the side surface during passing on the cylinder, then absorb and merge the vortex behind the downstream cylinder. This alternating impingement and reattachment generate large fluctuating forces to displace the downstream cylinder, leading to larger oscillations. The vortex shedding pattern behind the downstream cylinder appears as a relatively stable "P" mode, but there are a few SVs in it, which will affect the vortex shedding speed, causing the energy harvester to exhibit better performance only at specific high wind speeds (see Fig. 5). In summary, the CFD results interpret the physical insight of the performance enhancement or reduction of the proposed energy harvesting system and agree well with the above experimental results.

It should be mentioned that the two ash deposition types studied in this work are reasonable simplified. In fact, the shape of the ash deposited on the surface of the flue gas heat exchanger is constantly changing over time. The focus of future research is to combine this change to conduct more deeper application and theoretical research on wake galloping energy harvesters based on ash deposition effect.

4. Conclusions

This paper has explored the idea of deploying FIV-based energy harvesters in flue gas heat exchange devices for collecting electrical energy. The proposed system considers the ash deposition effect in the heat exchange system for the first time compared to the previously proposed wake galloping energy harvesting system. Bell-shaped and horn-shaped ash deposit cylinders have been designed according to the common ash deposition types. Wind tunnel experiments have been conducted to investigate the performance of the wake galloping piezoelectric energy harvester

(PEH) with different upstream ash deposit cylinders, at various space distances and under different wind speeds. It has been found that for compared to the horn-shaped cylinder, the bell-shaped cylinder is more beneficial for energy harvesting. Among all tested cases, the optimal configuration is determined to be the one with the bell-shaped ash deposition and the space ratio tuned to 1.5. In the optimal configuration, the threshold wind speed of the energy harvester is reduced, the effective wind speed range is widened, and the maximum voltage output is improved by over 111% than a conventional one operated in a traditional scenario.

The quenching phenomenon has been observed in the experiments when either shaped ash deposition adheres to the upstream cylinder. Through the fluid force analysis, the reason for the occurrence of the quenching phenomenon has been basically figured out. CFD studies have been conducted to reveal the underlying mechanisms to explain the experimental results. The simulation results clearly indicate that different ash deposit cylinders produce different wake vortices. Thus, the flow pattern changes with the space distance, which determines the dynamic response of the downstream cylinder and the voltage response of the bonded piezoelectric transducer. Compared with the existing wake energy harvesting system, the proposed system considers more practical applications in the field of thermal engineering. Especially in the harsh working environment that is difficult to access, solve the issue of sustainable power supply for wireless sensor nodes.

Credit author statement

Junlei Wang: Conceptualization, Methodology, Formal analysis, Software, Investigation, Writing − original draft. Chengyun Zhang: Methodology, Investigation, Data curation, Software, Visualization, Writing − original draft. Guobiao Hu: Conceptualization, Investigation, Supervision, Writing − review & editing. Xiaowei Liu: Supervision, Writing − review & editing. Huadong Liu: Writing − review & editing. Zhien Zhang: Writing − review & editing. Raj Das: Writing − review & editing

Declaration of competing interest

The authors declare that they have no known competing financial interests or personal relationships that could have appeared to influence the work reported in this paper.

Acknowledgements

References

[1] Gao M, Wang P, Jiang L, Wang B, Yao Y, Liu S, et al. Power generation for wearable systems. Energy Environ Sci 2021;14(4):2114−57.
[3] Yan B, Yu N, Ma H, Wu C. A theory for bistable vibration isolators. Mech Syst Signal Process 2022;167:108507.
[4] Lu Z, Zhao L, Ding H, Chen L. A dual-functional metamaterial for integrated vibration isolation and energy harvesting. J Sound Vib 2021;509:116251.
[5] Arionfard H, Nishi Y. Experimental investigation of a drag assisted vortex-induced vibration energy converter. J Fluid Struct 2017;68:48−57.
[7] Perez M, Boisseau S, Geisler M, Gasnier P, Willemin J, Despesse G, et al. Aeroelastic flutter energy harvesters self-polarized by triboelectric effects. Smart Mater Struct 2018;27(1):014003.

[8] Zhang C, Hu G, Yurchenko D, Lin P, Gu S, Song D, et al. Machine learning based prediction of piezoelectric energy harvesting from wake galloping. Mech Syst Signal Process 2021;160:107876.
[9] Chen G, Tang L, Yang Z, Tao K, Yu Z. An electret-based thermoacoustic-electrostatic power generator. Int J Energy Res 2020;44(3):2298−305.
[10] Wu Y, Li S, Fan K, Ji H, Qiu J. Investigation of an ultra-low frequency piezoelectric energy harvester with high frequency up-conversion factor caused by internal resonance mechanism. Mech Syst Signal Process 2022;162:108038.
[11] Li Z, Liu Y, Yin P, Peng Y, Luo J, Xie S, et al. Constituting abrupt magnetic flux density change for power density improvement in electromagnetic energy harvesting. Int J Mech Sci 2021;198:106363.
[12] Peng Y, Xu Z, Wang M, Li Z, Peng J, Luo J, et al. Investigation of frequency-up conversion effect on the performance improvement of stack-based piezoelectric generators. Renew Energy 2021;172:551−63.
[13] Wang M, Zhang J, Tang Y, Li J, Zhang B, Liang E, et al. Air-flow-driven triboelectric nanogenerators for self-powered real-time respiratory monitoring. ACS Nano 2018;12(6):6156−62.
[14] Bernitsas M, Raghavan K, Ben-Simon Y, Garcia E. VIVACE (vortex induced vibration aquatic clean energy): a new concept in generation of clean and renewable energy from fluid flow. Journal of Offshore Mechanics and Arctic Eng Trans ASME 2008;130(4):041101.
[15] Akaydin H, Elvin N, Andreopoulos Y. The performance of a self-excited fluidic energy harvester. Smart Mater Struct 2012;21(2):025007.
[16] Yang Y, Zhao L, Tang L. Comparative study of tip cross-sections for efficient galloping energy harvesting. Appl Phys Lett 2013;102(6):064105.
[17] Bryant M, Garcia E. Modeling and testing of a novel aeroelastic flutter energy harvester. J Vibr Acoustics-Trans ASME 2011;133(1):011012.
[18] Zhu H, Li G, Wang J. Flow-induced vibration of a circular cylinder with splitter plates placed upstream and downstream individually and simultaneously. Appl. Ocean Res 2020;97:102084.
[19] Sirohi J, Mahadik R. Harvesting wind energy using a galloping piezoelectric beam. J Vib Acoust 2011;134(1):011009.
[20] Zhang L, Dai H, Abdelkefi A, Wang L. Improving the performance of aeroelastic energy harvesters by an interference cylinder. Appl Phys Lett 2017;111(7):073904.
[21] Lv Y, Sun L, Bernitsas M, Sun H. A comprehensive review of nonlinear oscillators in hydrokinetic energy harnessing using flow-induced vibrations. Renew Sustain Energy Rev 2021;150:111388.
[22] Jafari M, Hou F, Abdelkefi A. Wind-induced vibration of structural cables. Nonlinear Dynam 2020;100(5):351−421.
[23] Jung H, Lee S, Jang D. Feasibility study on a new energy harvesting electromagnetic device using aerodynamic instability. IEEE Trans Magn 2009;45(10):4376−9.
[24] Usman M, Hanif A, Kim I, Jung H. Experimental validation of a novel piezoelectric energy harvesting system employing wake galloping phenomenon for a broad wind spectrum. Energy 2018;153:882−9.
[25] Zhou S, Wang J. Dual serial vortex-induced energy harvesting system for enhanced energy harvesting. AIP Adv 2018;8(7):075221.
[26] Abdelkefi A, Scanlon J, McDowell E, Hajj M. Performance enhancement of piezoelectric energy harvesters from wake galloping. Appl Phys Lett 2013;103(3):033903.
[27] Alhadidi A, Daqaq M. A broadband bi-stable flow energy harvester based on the wake-galloping phenomenon. Appl Phys Lett 2016;109(3):033904.
[28] Yan Z, Wang L, Hajj M, Yan Z, Sun Y, Tan T. Energy harvesting from iced-conductor inspired wake galloping. Extreme Mech Lett 2020;35:100633.
[29] Tamimi V, Wu J, Naeeni S, Shahvaghar-Asl S. Effects of dissimilar wakes on energy harvesting of Flow Induced Vibration (FIV) based converters with circular oscillator. Appl Energy 2021;281:116092.
[30] Yan Z, Shi G, Zhou J, Wang L, Zuo L, Tan T. Wind piezoelectric energy harvesting enhanced by elastic-interfered wake-induced vibration. Energy Convers Manag 2021;249:114820.
[31] Liu F, Zhang W, Zhao L, Zou H, Tan T, Peng Z, et al. Performance enhancement of wind energy harvester utilizing wake flow induced by double upstream flat-plates. Appl Energy 2020;257:114034.
[32] Jung H, Lee S. The experimental validation of a new energy harvesting system based on the wake galloping phenomenon. Smart Mater Struct 2011;20(5):055022.
[33] Zhu H, Gao Y, Hu J, Zhao H, Bao Y. Temporal-spatial mode competition in slug-flow induced vibration of catenary flexible riser in both in plane and out of plane. Appl Ocean Res 2022;119:103017.
[34] Abdelkefi A. Aeroelastic energy harvesting: a review. Int J Eng Sci 2016;100:112−35.
[35] Gao M, Cong J, Xiao J, He Q, Li S, Wang Y, et al. Dynamic modeling and experimental investigation of self-powered sensor nodes for freight rail transport. Appl Energy 2020;257:113969.
[36] Sun Y, Wang P, Lu J, Xu J, Wang P, Xie S, et al. Rail corrugation inspection by a self-contained triple-repellent electromagnetic energy harvesting system. Appl Energy 2021;286:116512.
[37] Tang S, He Y, Wang F, Tao Y. Parametric study on fouling mechanism and heat transfer characteristics of tube bundle heat exchangers for reducing fouling considering the deposition and removal mechanisms. Fuel 2018;211:301−11.
[38] Wacławiak K, Kalisz S. A practical numerical approach for prediction of particulate fouling in PC boilers. Fuel 2012;97:38−48.
[39] Cai Y, Kunlin T, Zheng Z, Yang W, Wang H, Zeng G, et al. Modeling of ash

formation and deposition processes in coal and biomass fired boilers: a comprehensive review. Appl Energy 2018;230:1447–544.

[40] Baxter L. Ash deposit formation and deposit properties. A comprehensive summary of research conducted at sandia's combustion research facility. office of scientific & technical information technical reports; 2000.

[41] Zhang L, Dai H, Abdelkefi A, Wang L. Experimental investigation of aerodynamic energy harvester with different interference cylinder cross-sections. Energy 2019;167:970–81.

[42] Hoffmann D, Folkmer B, Manoli Y. Fabrication, characterization and modelling of electrostatic micro-generators. J Micromech Microeng 2009;19(9):094001.

[43] Alam M, Moriya M, Takai K, Sakamoto H. Fluctuating fluid forces acting on two circular cylinders in a tandem arrangement at a subcritical Reynolds number. J Wind Eng Ind Aerod 2003;91(1–2):139–54.

[44] Alam M, Meyer J. Two interacting cylinders in cross flow. Phys Rev 2011;84(5 Pt 2):056304.

[45] Williamson C, Roshko A. Vortex formation in the wake of an oscillating cylinder. J Fluid Struct 1988;2(4):355–81.

[46] Tan Q, Fan K, Guo J, Wen T, Gao L, Zhou S. A cantilever-driven rotor for efficient vibration energy harvesting. Energy 2021;235:121326.

[47] Fan K, Hao J, Wang C, Zhang C, Wang W, Wang F. An eccentric mass-based rotational energy harvester for capturing ultralow-frequency mechanical energy. Energy Convers Manag 2021;241:114301.

[48] Wang J, Zhao L. Toward nonlinear galloping energy harvesting interfaced with different power extraction circuits. IEEE-ASME T Mech 2022. https://doi.org/10.1109/TMECH.2021.3121881.

[49] Yang K, Tong W, Lin L, Yurchenko D, Wang J. Active vibration isolation performance of the bistable nonlinear electromagnetic actuator with the elastic boundary. J Sound Vib 2022;520:116588.

[50] Yang K, Abdelkefi A, Li X, Mao Y, Dai L, Wang J. Stochastic analysis of a galloping-random wind energy harvesting performance on a buoy platform. Energy Convers Manag 2021;238:114174.

[51] Yan B, Pan X, Su R, Wu C. Nonlinear dynamics characteristics of a tumbler on an arc. J Sound Vib 2022;525:116810.

[52] Kan J, Wang J, Wu Y, Chen S, Wang S, Jiang Y, et al. Energy harvesting from wind by an axially retractable bracket-shaped piezoelectric vibrator excited by magnetic force. Energy 2022;240:122495.

[53] Kan J, Liao W, Wang J, Wang S, Yan M, Jiang Y, et al. Enhanced piezoelectric wind-induced vibration energy harvester via the interplay between cylindrical shell and diamond-shaped baffle. Nano Energy 2021;89:106466.

[54] Ma X, Zhou S. A review of flow-induced vibration energy harvesters. Energy Convers Manag 2022;254:115223.

[55] Chen W, Zhang Q, Li H, Hu H. An experimental investigation on vortex induced vibration of a flexible inclined cable under a shear flow. J Fluids Struct 2015;54:297–311.

[56] Liu Z, Li Y, Yang H, Na D, He Z. An accurate model of magnetic energy harvester in the saturated region for harvesting maximum power: analysis, design and experimental verification. IEEE T Ind Electron 2022. https://doi.org/10.1109/TIE.2022.3156033.

[57] Song R, Shan X, Lv F, Xie T. A study of vortex-induced energy harvesting from water using PZT piezoelectric cantilever with cylindrical extension. Ceram Int 2015;41:768–73.

[58] Shan X, Li H, Yang Y, Feng J, Wang Y, Xie T. Enhancing the performance of an underwater piezoelectric energy harvester based on flow-induced vibration. Energy 2019;172:134–40.

[59] Zhang H, Sui W, Yang C, Zhang L, Song R, Wang J. An asymmetric magnetic-coupled bending-torsion piezoelectric energy harvester: modeling and experimental investigation. Smart Mater Struct 2022;31:015037.

[60] Hou C, Li C, Shan X, Yang C, Song R, Xie T. A broadband piezo-electromagnetic hybrid energy harvester under combined vortex-induced and base excitations. Mech Syst Signal Process 2022;171:108963.

[61] Zhao L, Zou H, Zhao Y, Wu Z, Liu F, Wei K, et al. Hybrid energy harvesting for self-powered rotor condition monitoring using maximal utilization strategy in structural space and operation process. Appl Energy 2022;314:118983.

[62] Zou H, Zhao L, Wang Q, Gao Q, Yan G, Wei K, et al. A self-regulation strategy for triboelectric nanogenerator and self-powered wind-speed sensor. Nano Energy 2022;95:106990.

[63] Fang S, Zhou S, Yurchenko D, Yang T, Liao W. Multistability phenomenon in signal processing, energy harvesting, composite structures, and meta-materials: a review. Mech Syst Signal Process 2022;166:108419.